Cell Reports
Physical Science

CellPress
OPEN ACCESS

Article

Bottom-Up Fabrication of Oxygen Reduction Electrodes with Atomic Layer Deposition for High-Power-Density PEMFCs

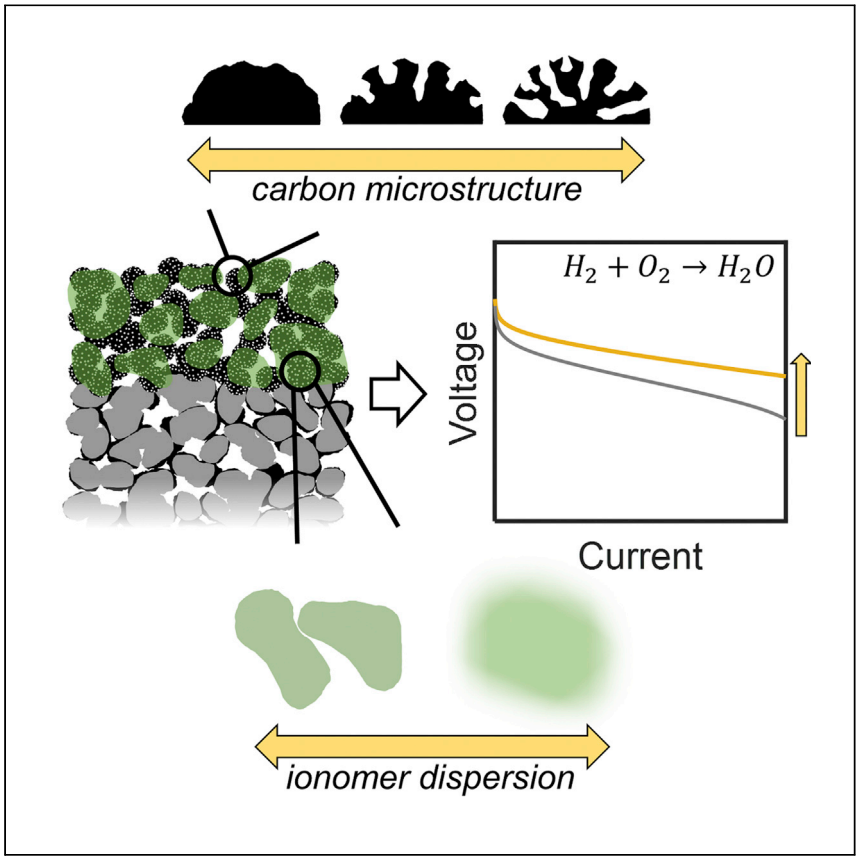

Proton exchange membrane fuel cell cathodes require new designs to reduce Pt content effectively. Here, Dull et al. introduce a bottom-up electrode fabrication architecture to study and optimize the catalyst microstructure. It is found that cathodes prepared with mesoporous furnace carbons and agglomerated ionomer dispersions deliver a notable fuel cell performance.

Samuel M. Dull, Shicheng Xu, Timothy Goh, ..., Jan Torgersen, Thomas F. Jaramillo, Fritz B. Prinz

johnxu@stanford.edu (S.X.)
jaramillo@stanford.edu (T.F.J.)
fprinz@stanford.edu (F.B.P.)

HIGHLIGHTS

Fuel cell cathode fabrication with sequential deposition of carbon, Pt, and ionomer

Mesoporous carbon and ionomer agglomerates minimize ionomer exposure to Pt

Strong oxygen reduction performance at both low and high current densities

Dull et al., Cell Reports Physical Science 2, 100297
January 20, 2021 © 2020
https://doi.org/10.1016/j.xcrp.2020.100297

Cell Reports
Physical Science

CellPress
OPEN ACCESS

Article

Bottom-Up Fabrication of Oxygen Reduction Electrodes with Atomic Layer Deposition for High-Power-Density PEMFCs

Samuel M. Dull,[1,2] Shicheng Xu,[3,*] Timothy Goh,[4] Dong Un Lee,[1,2] Drew Higgins,[5] Marat Orazov,[6] David M. Koshy,[1,2] Per Erik Vullum,[7] Sebastian Kirsch,[8] Gerold Huebner,[8] Jan Torgersen,[9] Thomas F. Jaramillo,[1,2,*] and Fritz B. Prinz[3,4,9,10,*]

SUMMARY

As the platinum (Pt) loading in proton exchange membrane fuel cell cathodes is driven down to reduce costs, catalyst utilization becomes increasingly important. Here, we report an atomic layer deposition-facilitated electrode fabrication technique designed to improve the catalyst-ionomer interface. The ionomer solvent environment and carbon support nanoporosity are studied independently, and it is found that the combination of an agglomerated ionomer dispersion and a mesoporous support gives access to a high catalytic activity (mass activity [MA] = 0.31 A/mg_{Pt} with pure Pt) that can be maintained at high current densities. We hypothesize that the formulation results in Pt sufficiently withdrawn from the ionomer such that poisoning and transport losses are reduced. When paired with a low-resistance dispersion-cast membrane, a 0.1-mg_{Pt}/cm^2 cathode can deliver a 0.65-V power density of 1.0 W/cm^2 at 150 kPa and 80°C. The assembly also demonstrates impressive durability, losing only 33 mV after 30,000 cycles.

INTRODUCTION

Enabling fast refueling and long ranges,[1] hydrogen (H_2)-powered proton exchange membrane fuel cells (PEMFC) are emerging alongside lithium (Li)-based batteries as a reduced-emission alternative to internal combustion engines (ICEs) for transportation applications. To lower costs and support the deep market penetration of PEMFC vehicles, automotive manufacturers are interested in decreasing the quantity of platinum (Pt) in the electrodes.[2] For reference to the incumbent technology, ICE vehicles also use scarce and expensive Pt-group metals (PGM) in catalytic converters, but only use 2–8 g compared to the ≥30 g in the latest fuel cell vehicles.[2] Aligned with the aims of automotive manufacturers, the US Department of Energy (DOE) has set a total areal loading target of 0.125 mg_{PGM}/cm^2, equivalent to ~11.3 g_{PGM} for a midsized, 90 kW_{gross} vehicle.[3]

Because of the rapid H_2 oxidation kinetics on Pt catalysts, anode loadings as low as 0.025 mg_{Pt}/cm^2 can be used in PEMFCs without considerable voltage loss.[4–6] This leaves a target of <0.1 mg_{Pt}/cm^2 for the cathode to achieve the rated power density of 1 W/cm^2 at a reasonable cell efficiency.[3] Due to sluggish oxygen (O_2) reduction reaction (ORR) kinetics and the relatively dilute presence of O_2 in air, this presents a major challenge. To improve ORR kinetics, a large body of important work has gone into improving the intrinsic activity of Pt, largely through alloying[7,8] and

[1]Department of Chemical Engineering, Stanford University, Stanford, CA 94305, USA

[2]SUNCAT Center for Interface Science and Catalysis, SLAC National Accelerator Laboratory, Menlo Park, CA 94025, USA

[3]Department of Mechanical Engineering, Stanford University, Stanford, CA 94305, USA

[4]Department of Material Science and Engineering, Stanford University, Stanford, CA 94305, USA

[5]Department of Chemical Engineering, McMaster University, Hamilton, ON L8S 4L8, Canada

[6]Department of Chemical and Biomolecular Engineering, University of Delaware, Newark, DE 19716, USA

[7]SINTEF, Trondheim 7465, Norway

[8]Volkswagen Group Research, Wolfsburg, Germany

[9]Department of Mechanical and Industrial Engineering, Norwegian University of Science and Technology, Trondheim 7491, Norway

[10]Lead Contact

*Correspondence: johnxu@stanford.edu (S.X.), jaramillo@stanford.edu (T.F.J.), fprinz@stanford.edu (F.B.P.)

https://doi.org/10.1016/j.xcrp.2020.100297

nanostructuring.[9,10] Although order-of-magnitude improvements have been made in mass-normalized activity relative to Pt in the rotating disk electrode test configuration,[11] translating these improvements into industrially relevant membrane electrode assemblies (MEAs) has remained a challenge. Furthermore, while the theoretical voltage loss upon reducing the cathode loading from 0.3 mg_{Pt}/cm^2 to 0.1 mg_{Pt}/cm^2 is only ~33 mV for a given Pt catalyst,[2] additional voltage losses are observed at high current densities (HCDs) due to the depletion of O_2 at the Pt surface.[2] These transport-related losses are independent of intrinsic catalyst activity and can exceed 100 mV for low-loaded cathodes at HCDs.[2]

Engineering the Pt-ionomer interface in the cathode is a broad research strategy that can both mitigate transport losses and improve catalytic activity. The ionomer, while necessary for delivering protons to the Pt surface, impedes O_2 transport[2,12] and can act as a catalyst poison.[13,14] For this reason, minimizing the exposure of Pt to the ionomer while maintaining sufficiently high proton accessibility is crucial to PEMFC performance. In the traditional fabrication of an MEA, Pt is synthesized on a carbon support and mixed with an ionomer dispersion to form an ink that is subsequently cast onto either the membrane or gas diffusion media.[15] Characterizing the Pt-ionomer interface that results from this preparation is difficult, but recent research has shown that the interface may be sensitive to experimental parameters such as Pt synthesis technique,[16] ionomer molecular structure,[17–19] dispersant/solvent composition,[20–23] ink dispersion technique,[24] carbon surface functionalization,[25,26] and carbon pore size distribution.[5,27]

Despite the strong results achieved through optimization within this fabrication framework, it is important to identify alternative preparation routes that may be subject to different practical constraints. For example, in the traditional ink-based architecture, certain solvent compositions and sonication/stirring procedures are needed to properly disperse the solids for film application. Here, we introduce an MEA fabrication technique facilitated by atomic layer deposition in which carbon, Pt, and ionomer are deposited sequentially. Unconstrained by the need to disperse an ink, we can tune the ionomer solvent environment independently of the Pt/carbon nanostructure. In evaluating a series of ionomer dispersion alcohol contents and carbon supports, we found that the combination of agglomerated ionomer dispersions and mesoporous furnace carbons yielded remarkably active cathodes at both low current densities (LCDs) and HCDs. When used in conjunction with a low-resistance dispersion-cast membrane, power densities of 1.0 and 1.3 W/cm^2 at 0.65 V could be obtained in air under differential flow at 150 and 230 kPa backpressures, respectively. Per the US DOE protocol, the MEA was also subjected to 30,000 square-wave cycles between 0.6 and 0.95 V to assess its durability. In line with the targeted 30 mV loss as 0.8 and 1.5 A/cm^2, the assembly lost 21 and 33 mV at those respective current densities after degradation.

RESULTS

Electrode Fabrication and Electrochemical Characterization

In our bottom-up electrode fabrication (depicted in Figure 1), an ~2- to 5-μm layer of carbon is deposited onto the microporous layer of a gas diffusion layer via vacuum filtration[28] (Figure 1A). Pt is then grown on the carbon using 30 cycles of a CO-passivated atomic layer deposition (PALD) recipe[29] (Figure 1B). While in principle this Pt/carbon layer could be prepared without ALD, it is practically difficult to form such a thin layer from a Pt/carbon powder without introducing an ionomer for its dispersing and adhesion properties. Furthermore, we previously demonstrated that PALD Pt delivers heightened activity and durability due to the flattened geometry and

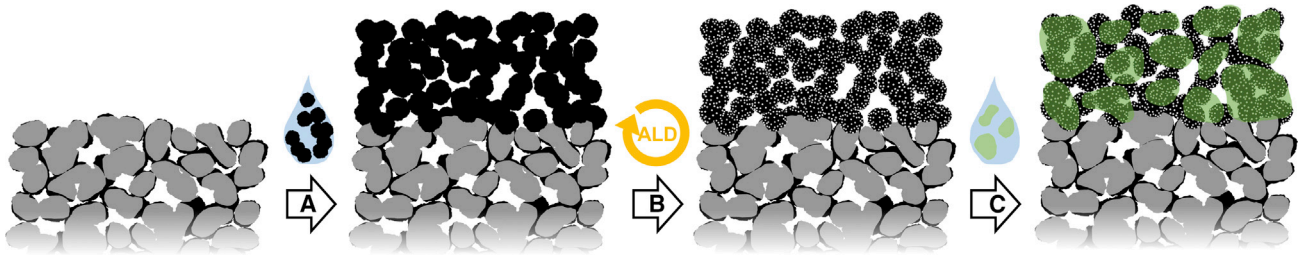

Figure 1. Schematic Illustration of the Bottom-Up Electrode Fabrication Procedure

(A) Carbon deposited on the polytetrafluoroethylene (PTFE)-treated microporous layer of the gas diffusion media via vacuum filtration.

(B) Pt nanoparticles deposited on the carbon layer via atomic layer deposition (ALD).

(C) The Pt/carbon layer impregnated with an ionomer dispersion via drop casting.

uniform size of the resulting Pt particles.[29] To conclude the fabrication process, the catalyst layer is impregnated with ionomer by drop casting a dilute ionomer dispersion onto the surface (Figure 1C). For studying the effects of ionomer dispersant and carbon support, cathodes were assembled with commercial 0.1 mg_{Pt}/cm^2 anode-coated membranes for testing. As discussed later in more detail, a cast membrane[30] was prepared for power density measurements. The ALD-prepared MEAs were conditioned and tested under differential flow at 80°C, 100% relative humidity (RH), and 150 kPa backpressure, unless otherwise noted.

A major goal of this work was to assess the catalytic performance of cathodes across a wide range in current density. The most common metric reported for ORR kinetics in PEMFCs is the mass-normalized current at an iR-corrected cell potential of 0.9 V.[31] Because transport-related losses at this cell potential are negligible, this "mass activity" (MA) is used to describe the kinetics of ORR in the cathode. However, current densities relevant to high-power fuel cell operation are nearly two orders of magnitude greater than those measured for the MA. At these current densities, voltage losses after standard ohmic and concentration[32] corrections are commonly observed[16,25] that cannot be accounted for by simple (i.e., fixed slope) Tafel kinetics.[33] Mechanistic studies[34,35] building from the double trap kinetic model[36] attribute these losses to the increasing Tafel slope associated with potential-dependent changes in surface oxide coverage. The probable inaccuracy in determining concentration losses with limiting current measurements is also often considered.[16,25] Regardless of their exact origin, these unexplained losses vary in quantity depending on the catalytic environment of the cathode. Here, we define catalyst utilization at HCDs (U_{HCD}) as the H_2 crossover-corrected current density (i_{eff}) at an ohmic- and concentration-corrected cell potential of 0.75 V normalized by the current density projected from 0.85 V, assuming simple Tafel kinetics (Equation 1):

$$U_{HCD}(\%) = \frac{i_{0.75V}}{i^{Tafel,\ 0.85V}_{0.75V}} x100\% \qquad \text{(Equation 1)}$$

With the kinetic current density ~27 times greater at 0.75 V than at 0.85 V under this assumption, U_{HCD} quantifies unattributed voltage losses that evolve from the LCD regime to the HCD regime. Therefore, while MA defines the LCD performance of the catalyst, U_{HCD} describes the HCD performance. We also include the total O_2 transport resistance[37,38] in assessing HCD performance, but note that the value is loading dependent and tends to correlate with U_{HCD}.

Effects of Ionomer Dispersant on Electrochemical Performance

To assess the effect of ionomer dispersant composition on MEA performance, aqueous Nafion formulations with different total alcohol content—0, 7.8, 15.6,

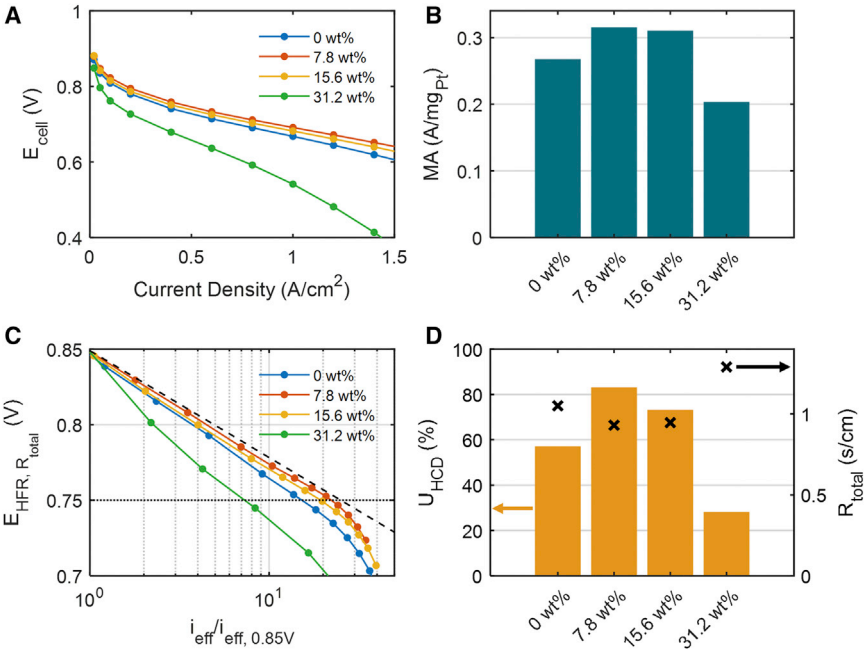

Figure 2. Effect of Ionomer Dispersion Alcohol Content on Fuel Cell Performance

(A) Uncorrected MEA H_2-air polarization curves for cathodes prepared with ionomer dispersions containing different alcohol concentrations.

(B) MEA H_2-O_2 mass activity (MA) values.

(C) MEA H_2-air polarization curves with potentials corrected for high-frequency resistance (HFR) and total O_2 transport resistance (R_{total}) and current densities corrected for H_2 crossover and normalized by the value at 0.85 V. The dashed line represents a theoretical curve following simple Tafel kinetics.

(D) High current density catalyst utilization (U_{HCD}) values (left) extracted from (C) and R_{total} values (right).

Conditions: active area = 5 cm^2; cathode loading = 0.095 $\pm$ 0.015 mg_{Pt}/cm^2; anode loading = 0.1 mg_{Pt}/cm^2; cell temperature = 80°C; total outlet pressures = 150 kPa; cathode and anode RH = 100%; cathode flow rate = 5,000 sccm; anode flow rate = 500 sccm.

and 31.2 wt%—were prepared via dilution with n-propanol and used to impregnate catalyst layers prepared with PALD Pt and a porous carbon black (CB-KB, discussed later). Cathodes with loadings of 0.095 $\pm$ 0.015 mg_{Pt}/cm^2 were fabricated in this way and tested under the aforementioned conditions. Figure 2A displays the uncorrected polarization curves corresponding to each ionomer dispersion. Evidently, the 0 wt% alcohol sample trails slightly behind the intermediate 7.8 and 15.6 wt% samples, while the 31.2 wt% sample performs significantly worse. LCD and HCD performances are formalized in Figures 2B and 2D. MA (Figure 2B) reaches a respectable ~0.31 A/mg_{Pt} for the intermediate 7.8 and 15.6 wt% alcohol samples, followed by 0.27 and 0.20 for the 0 and 31.2 wt% samples, respectively. U_{HCD} values displayed in Figure 2D were extracted from the corrected and normalized polarization curves (Figure 2C). With a U_{HCD} of ~83%, the 7.8 wt% sample retained a significant portion of its LCD catalytic performance in the HCD regime; the 15.6, 0, and 31.2 wt% samples followed in that order. The total transport resistances (R_{total}) (Figure 2C) are inversely correlated with the U_{HCD} values for the dataset, pointing to the shortcomings in describing concentration losses with limiting current measurements.

With increasing alcohol content under 50 wt%, solvent properties such as viscosity[39] and surface tension[40] change monotonically. Because we observe an intermediate concentration being optimal for MEA performance, these factors alone are unlikely

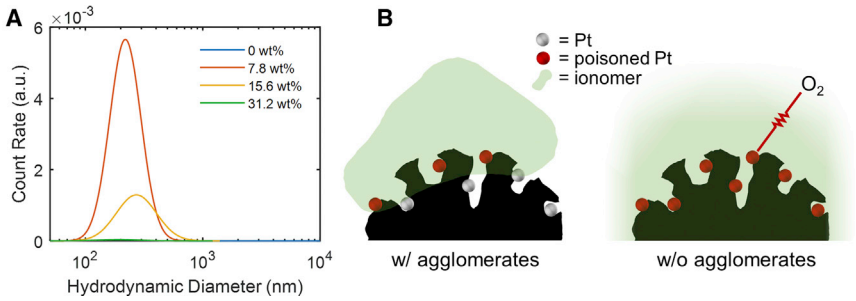

Figure 3. Physical Characterization of Ionomer Dispersions

(A) Dynamic light scattering measurements for 0.5 wt% ionomer dispersions containing different alcohol concentrations.

(B) Illustration of the hypothesized catalyst nanostructures formed with agglomerated and non-agglomerated ionomer dispersions.

to provide a complete explanation of the electrochemical results. Another process that is sensitive to solvent composition is the formation of ionomer agglomerates. It is generally known that water-alcohol mixtures disperse proton-conducting ionomers in large, swollen agglomerates,[20,22,41] but the exact morphologies and sizes of these agglomerates for a given solvent environment are difficult to predict.[41] Here, we observe the formation of Nafion agglomerates at the intermediate 7.8 and 15.6 wt% alcohol dispersions. Interactions of the agglomerates with light are visible to the naked eye, as shown in Figure S1, and can be quantified using dynamic light scattering (DLS). Figure 3A shows the scattering intensities for each ionomer dispersion as a function of hydrodynamic diameter. Peaks between 200 and 250 nm are pronounced for the intermediate alcohol dispersions, but very little scattering is observed for the 0 and 31.2 wt% solutions. Thus, according to our electrochemical data, the presence of Nafion agglomerates in the ionomer dispersion is associated with higher catalytic performance. We hypothesize that the enhancement originates from a reduced exposure of Pt to the ionomer. In agglomerates, polymer strands have a greater affinity for each other than the surrounding dispersing molecules. Therefore, as we depict in Figure 3B, Nafion in agglomerates would be less driven to follow the solvent into the nanometer-scale pores in which Pt is located. Because ionomer is known to both poison Pt[13,14] and add O_2 transport resistances,[2,12] increased penetration for non-agglomerated dispersions would reduce both LCD and HCD performance. As for the poor performance for the 31.2 wt% sample relative to the 0 wt% sample, the reduced surface tension of the high-alcohol dispersion likely further increases ionomer penetration. This factor may also explain the slight reduction in performance of the 15.6 wt% sample relative to the 7.8 wt% sample.

With agglomerated dispersions, we can achieve relatively high activities and account for ~83% of voltage losses observed below roughly 1.5 A/cm^2. Retention of simple Tafel kinetics at high current densities is a major challenge in PEMFC research, especially for porous carbons with high activities.[16] In accordance with the results presented here, we theorize that the strong HCD results can be attributed to the incorporation of agglomerated ionomer via a water-heavy (i.e., high surface tension) dispersion.

Effects of Carbon Nanoporosity on Electrochemical Performance

To examine the effects of support on PEMFC performance[5,25–27] within the bottom-up MEA fabrication framework, we evaluated three furnace CBs with varying degrees of porosity (CB-V, CB-KB, and CB-KBHSA) and one ordered mesoporous carbon (OMC)

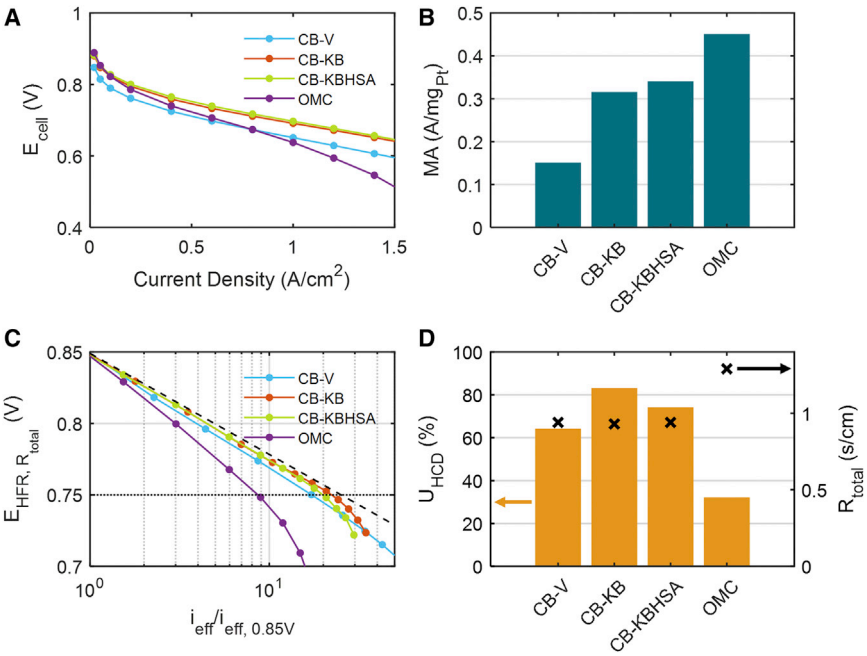

Figure 4. Effect of Carbon Support Structure on Fuel Cell Performance

(A) Uncorrected MEA H_2-air polarization curves for cathodes prepared with different carbon supports.

(B) MEA H_2-O_2 MA values.

(C) MEA H_2-air polarization curves with potentials corrected for HFR and total O_2 transport resistance (R_{total}) and current densities corrected for H_2 crossover and normalized by the value at 0.85 V. The dashed line represents a theoretical curve following simple Tafel kinetics.

(D) U_{HCD} values extracted from (C) (left) and R_{total} values (right).

Conditions: active area = 5 cm^2; cathode loading = 0.10 ± 0.02 mg$_{Pt}$/cm^2; anode loading = 0.1 mg$_{Pt}$/cm^2; cell temperature = 80°C; total outlet pressures = 150 kPa; cathode and anode RH = 100%; cathode flow rate = 5,000 sccm; anode flow rate = 500 sccm.

with channels templated at ~4.5 nm in diameter. Figure 4 contains the fuel cell testing results for 0.10 ± 0.02 mg$_{Pt}$/cm^2 loaded cathodes fabricated with each carbon and the 7.8 wt% alcohol Nafion dispersion from the ionomer study. Consistent with the prior literature, CB-V-supported Pt demonstrated a lower MA than CB-KB.[5] The more porous CB-KBHSA revealed a slightly higher LCD performance than CB-KB, with an MA of 0.34 A/mg$_{Pt}$. Finally, Pt supported on the OMC resulted in the highest MA, reaching 0.45 A/mg$_{Pt}$ and thereby exceeding the US DOE target of 0.44 A/mg$_{Pt}$.[3]

According to the transmission electron microscopy (TEM) analysis presented in Figure S2, Pt deposition by PALD resulted in ~3 nm particles on each carbon support, with differences small enough that the effects of particle size on activity[42] can be neglected when comparing between the supports. In recent work demonstrating a positive correlation between MEA performance and support mesoporosity, it was argued that 4–7 nm pores are large enough not to be blocked by Pt nanoparticle growth but small enough that ionomer penetration is low.[5] Following this perspective, we define f_{4-7nm} for each carbon as the fraction of total surface area contained within 4–7 nm pores. Assuming Pt nanoparticles nucleate uniformly across the carbon surface, f_{4-7nm} describes the fraction of Pt located within pores that ostensibly have restricted ionomer access. When MA is plotted against f_{4-7nm} (Figure 5B, closed circles), a clear trend is observed. We acknowledge here that a significant portion of surface area in CB-KB and CB-KBHSA belongs to pores between 3.5

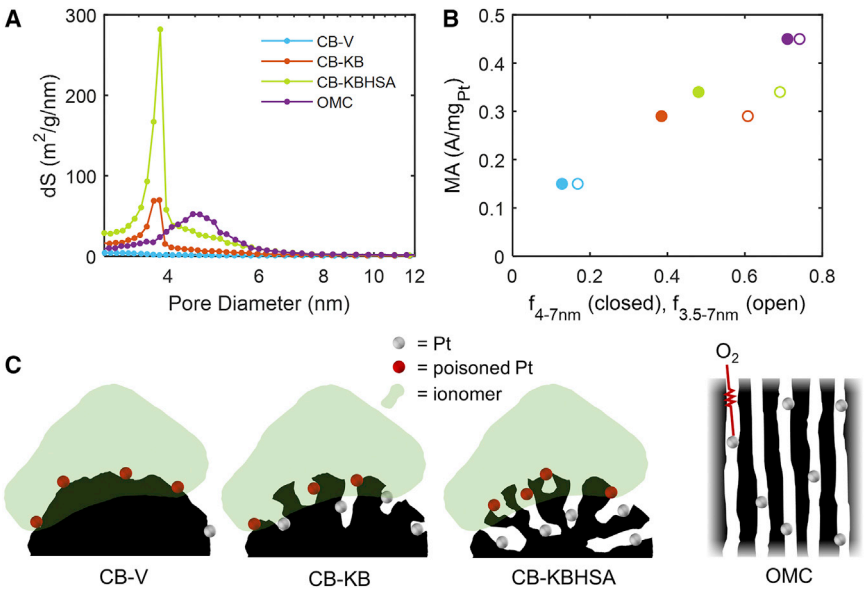

Figure 5. Physical Characterization of Carbon Supports

(A) Pore size distribution curves calculated from N_2 desorption curves using Barrett-Joyner-Halenda theory.

(B) MA values plotted against the fractions of support surface area contained in 4–7 nm and 3.5–7 nm pores.

(C) Illustration of the hypothesized catalyst nanostructures for each carbon.

and 4 nm (isotherms are displayed in Figure S3). While in principle Pt contained in these pores should not have reduced activity—unless Pt nucleation changes as the pore diameter approaches the nominal nanoparticle size—the 4- to 7-nm size range was selected following the precedent in the literature. In any case, a monotonic relationship between degree of mesoporosity and MA holds if the size range is adjusted (Figure 5B, open circles), albeit with a weaker correlation.

The degree of mesoporosity did not, however, predict the trend in HCD performance. The OMC, for example, yielded the lowest U_{HCD} by a significant margin despite having >60% of surface area in 4–7 nm pores. We believe that this poor performance is caused primarily by the large primary particle size characteristic of OMCs. With long channels on the order of 1 μm, O_2 accessibility and water removal are presumably challenges, highlighting pore length as a key factor in HCD performance. Although pore length is challenging to measure, we can make assumptions based on the size and geometries of the carbon species tested to better understand the relationship. That is, because all of the furnace CBs (CB-V, CB-KB, CB-KBHSA) have 30–50 nm spherical primary particles, differences in mesoporosity should roughly translate into differences in pore length within the primary particles (as depicted in Figure 5C). With no pronounced mesoporosity (see Figure 5A), CB-V supports Pt predominantly on its surface. Bulk O_2 transport seems unhindered by the resulting exposure to ionomer (R_{total} is low for XC-72), but U_{HCD} suffers slightly. Pt deposited on CB-KB and CB-KBHSA, however, seems to be withdrawn enough that only minor unexplained losses are observed but not so much that the diffusion length of O_2 is considerably increased. The slightly lower U_{HCD} of CB-KBHSA compared to CB-KB may suggest that the optimum pore length was surpassed for the more porous carbon.

Among the CBs tested, CB-KB produced the lowest total O_2 transport resistance (R_{total} = 0.93 s/cm) and the greatest retention of activity (U_{HCD} = 83%). Although

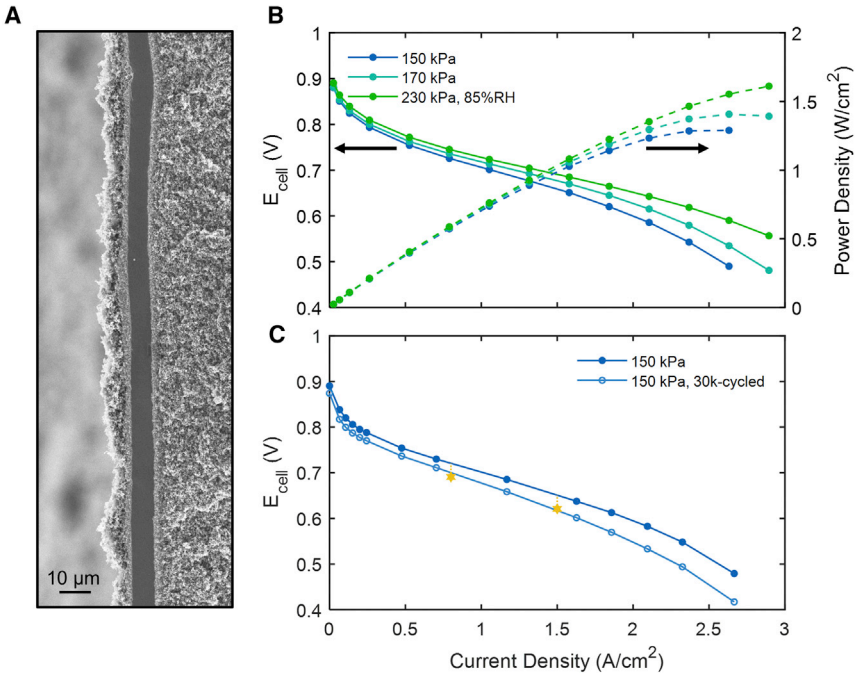

Figure 6. Electrochemical Measurements Using a Dispersion-Cast Membrane

(A) Scanning electron microscopy (SEM) image of the cross-section of an MEA prepared with a dispersion cast membrane; the membrane, observable as a dark band down the center, is flanked by the catalyst layers of the anode (left) and the cathode (right).

(B) Uncorrected MEA H_2-air polarization curves taken at various backpressures using a cast membrane; the 85% RH condition in the 230 kPa case was selected to minimize flooding.

Conditions: active area = 3.8 cm^2; cathode loading = 0.10 mg_{Pt}/cm^2; cell temperature = 80°C; cathode flow rate = 5,000 sccm; anode flow rate = 500 sccm.

(C) Uncorrected MEA H_2-air polarization curves taken before and after 30,000 square-wave cycles between 0.6 and 0.95 V with 3-s holds at each potential. The gold stars correspond to the 30-mV loss targeted by the US DOE.

Conditions: active area = 3.5 cm^2; cathode loading = 0.12 mg_{Pt}/cm^2; cell temperature = 80°C; cathode flow rate = 5,000 sccm; anode flow rate = 1,000 sccm.

the MA over CB-KB is respectable for pure Pt at 0.31 A/mg_{Pt}, significantly higher MA values are attainable as demonstrated with the OMC tested. According to our hypotheses, a carbon with a large proportion of relatively shallow mesopores could reconcile the observed trade-off between LCD and HCD performance.

Power Density and Durability Measurements with a Low-Resistance Cast Membrane

After the kinetic voltage losses described by MA and U_{HCD}, ohmic drops are the greatest source of efficiency loss in PEMFCs until O_2 transport losses become more significant at well over 2 A/cm^2. For this reason, a highly conductive membrane is essential for achieving the rated power density at a reasonable efficiency. It has previously been shown that preparing membranes by casting an ionomer dispersion directly onto the electrodes not only reduces the membrane resistance to the level of electrical resistances in the cell[30] but also decreases the O_2 transport resistance, possibly due to back diffusion of water to the anode.[43]

Here, a ~6-μm membrane (Figure 6A) was prepared on the anode[30,43] and assembled with a 0.1-mg_{Pt}/cm^2 cathode fabricated using CB-KB and the 7.8 wt% alcohol Nafion dispersion. With the introduction of this cast membrane, the total transport resistance

decreased to 0.85 s/cm (Figure S4B) and the cell resistance measured by high-frequency impedance decreased to roughly 40 mOhm-cm^2 (Figure S4A), a low but not unprecedented value.[25,30] Polarization curves taken at common absolute backpressures of 150, 170, and 230 kPa are displayed in Figure 6B along with their corresponding power densities. The commercial relevance of testing at higher backpressures is that the power density increase from more favorable thermodynamics, kinetics, and transport may outweigh the equipment and energy cost for compressing the air feed.[44] Here, we observe for the 3 pressures power densities at 0.65 V of 1.0 W/cm^2, 1.15 A/cm^2, and 1.3 W/cm^2, respectively. The selected cell potential of 0.65 V defines what is generally regarded as the minimum cell efficiency of interest to commercial PEMFCs. To the best of our knowledge, these power densities are among the highest reported at the respective backpressures for cathode loadings less than or equal to the target loading of 0.1 mg/cm^2. Polarization curve reproducibility is demonstrated with 3 samples in Figure S5, and comparisons to other literature are made in Table S1.

To assess the durability of an MEA fabricated with bottom-up ALD electrodes and a cast membrane, 30,000 square-wave cycles between 0.6 and 0.95 V were carried out per the US DOE accelerated degradation protocol. The resulting polarization curve shown in Figure 6C demonstrates a downward shift after cycling, which is expected for a finite loss of active catalytic material. Nonetheless, the voltage losses of ~21 and 33 mV at 0.8 A/cm^2 and 1.5 A/cm^2 are within the range of the 30 mV targeted by the US DOE,[3] as marked with gold stars in Figure 6C. We have previously demonstrated the enhanced durability of PALD-prepared Pt in a rotating disk electrode (RDE) configuration.[29] Compared to a commercial Pt supported on high-surface-area carbon, PALD Pt lost nearly 30% less electrochemically active catalyst through 10,000 voltage cycles between 0.6 and 1.0 V. This improvement is credited to the smaller particle size variation and greater interparticle spacing, which make the Pt less susceptible to Ostwald ripening and agglomeration, for Pt prepared with PALD. Additional explanations for the impressive MEA durability presented here may involve a favorable positioning of Pt nanoparticles with respect to the ionomer[21] and carbon pores,[45] and a deeper investigation into these possibilities is warranted. For reference, durability data from selected literature are tabulated in Table S2.

DISCUSSION

In addition to delivering high-performing PEMFCs, we anticipate that our bottom-up fabrication strategy for leveraging ionomer control will be generally useful to other gas diffusion electrode-driven fields; the approach may be particularly attractive to those working in CO_2 electroreduction, in which the catalyst-ionomer interface has an additional effect in product selectivity.[46] Furthermore, by using ALD to prepare the Pt, we demonstrated the feasibility of making electrodes using vapor-based synthesis on high surface area substrates without involving fluidization[47] or agitation.[48] The recent development of spatial ALD reactors[49] could make this electrode fabrication methodology a feasible commercial alternative to conventional approaches.

EXPERIMENTAL PROCEDURES

Resource Availability

Lead Contact

Further information and requests for resources should be directed to and will be fulfilled by the lead contact, F.B.P. (fprinz@stanford.edu).

Materials Availability

This study did not generate new unique reagents.

Data and Code Availability

The authors declare that the data supporting the findings of this study are available within the article and the Supplemental Information. All other data are available from the Lead Contact upon reasonable request.

Membrane Electrode Assembly Fabrication

All cathodes were prepared following the process depicted in Figure 1. Using a filtration process,[28] carbon dispersed in alcohol was deposited as a ~2- to 4-μm layer (~0.1–0.2 mg/cm^2) onto a Sigracet 29BC gas diffusion layer. Before Pt deposition, the sample was treated for 10 min with O_2 plasma (Harrick PDC-001, 30 W) to functionalize the carbon. PALD was conducted with the procedure specified in our previous publication.[29] Pt loadings were determined by measuring the Pt Lα X-ray fluorescence signal (SPECTRO XEPOS spectrometer HE) and interpolating the areal loading from a calibration curve. The resulting catalyst layers were saturated (nominally an ionomer:carbon weight [I:C] ratio of 4) with the selected 0.5 wt% Nafion dispersion as specified below. To prepare the 0 wt% alcohol dispersion, 10 wt% 1100 EW Nafion in pure water was diluted with ultrapure water (18.2 mΩ-cm, total organic carbon [TOC] < 5 ppb). The 7.8, 15.6, and 31.2 wt% alcohol dispersions were prepared by diluting a 5 wt% 1100 EW Nafion dispersed in lower aliphatic alcohols and 15–20 wt% water with ultrapure water and n-propanol (J.T. Baker). For the ionomer and carbon studies, cathodes were cut to 5 cm^2 and assembled with a commercial anode-coated membrane. For the power density measurements, the membranes and anodes were prepared in-house. Cathodes were cut to areas of ~4 cm^2, and these areas were measured precisely to define the active area. A schematic of the assembly process is shown in Figure S6.

Electrochemical Characterization

MEA testing was done in a Scribner 840 fuel cell testing system using a Greenlight 50 cm^2 research cell fixture with a serpentine flow pattern. Cell compression was set to 4 bars and, unless otherwise stated, cells were maintained at 80°C, 100% RH, and 150 kPa absolute backpressure. After activation and before all polarization curve measurements, a cathode recovery step was carried out.[50] Cyclic voltammograms were taken at several points during the testing protocol with the cathode purged with Ar (99.999%, Praxair). The average of the cathodic and anodic currents in the capacitive region provided the parasitic H_2 crossover current. For activity measurements, O_2 (99.993%, Praxair) and H_2 (99.999%, Praxair) were fed at 5,000 sccm and 500 sccm, respectively. For each cell potential (0.82, 0.85, 0.88, 0.89, and 0.90 V), current densities were measured at the end of 5 min.[51–53] The limiting current was recorded as the average current density during the brief 0.3-V hold across all of the measurements.[38] Polarization curves were taken in 5,000 sccm house air with currents held for 3 min, per the US DOE protocol.[3] The cell resistance used to calculate ohmic losses was taken from the high-frequency x-intercept of an electrochemical impedance Nyquist plot measured at 0.25 A in O_2. Impedance fitting revealed negligible proton resistance within the catalyst layer for all of the samples at the conditions tested. The accelerated degradation (30,000 square-wave cycles between 0.6 and 0.95 V with 3-s holds at each potential) was carried out in 1,000 sccm H_2 and 5000 sccm N_2 at 80°C, 100% RH, and 150 kPa absolute backpressure. In post-processing, the limiting current was used to calculate the total O_2 transport resistance[37] and concentration voltage losses as a function of current density.[32]

DLS

Hydrodynamic diameters for each ionomer dispersion were measured using Brookhaven's NanoBrook Omni. Aliquots of ~2 mL were analyzed at 25°C in the 90° angle configuration with a maximized count rate. Volume-transformed size distributions were weighted by count rate to compare the relative extent of agglomeration between the dispersions.

N_2 Sorption

N_2 physisorption measurements were taken in a Quantachrome Instruments Autosorb-IQ. After degassing ~100 mg plasma-treated carbon at 150°C for 3 h, adsorption and desorption isotherms were recorded at 77 K in the P/P_0 range 0.025–0.995. Pore size distributions were calculated using the Brunauer-Emmett-Teller (see Figure S3B) and Barrett-Joyner-Halenda methods, respectively.

Imaging

A cryo-fractured cross-section of the cast membrane MEA was imaged in a FEI Magellan 400 XHR scanning electron microscope using an accelerating voltage of 5 kV and a beam current of 50 pA. TEM imaging was performed with a double Cs aberration-corrected cold FEG JEOL ARM 200F, operated at 200 kV.

SUPPLEMENTAL INFORMATION

Supplemental Information can be found online at https://doi.org/10.1016/j.xcrp.2020.100297.

ACKNOWLEDGMENTS

This work was supported financially by the Volkswagen Group of America. Part of the work was performed at the Stanford Nano Shared Facilities (SNSF), supported by the National Science Foundation under award ECCS-1542152. The TEM work was carried out on NORTEM infrastructure, grant 197405, TEM Gemini Centre, Norwegian University of Science and Technology (NTNU), Norway.

AUTHOR CONTRIBUTIONS

S.X. conceived of the ALD electrode bottom-up fabrication architecture. S.M.D. and S.X. designed the ionomer formulation study. S.M.D., S.X., and D.M.K. designed the carbon support structure study. S.M.D., S.X., T.G., D.U.L., and M.O. carried out the preliminary membrane electrode assembly tests, with the guidance of D.H., S.K., and G.H. S.M.D. performed the material characterization and analysis. S.M.D., S.X., T.G., D.U.L., D.H., D.M.K., T.F.J., and F.B.P. wrote the manuscript.

DECLARATION OF INTERESTS

The authors declare the pending US Patent 16/791,650.

Received: August 29, 2020
Revised: October 27, 2020
Accepted: December 1, 2020
Published: January 11, 2021

REFERENCES

1. Gröger, O., Gasteiger, H.A., and Suchsland, J.-P. (2015). Review—Electromobility: Batteries or Fuel Cells? J. Electrochem. Soc. *162*, A2605–A2622.

2. Kongkanand, A., and Mathias, M.F. (2016). The Priority and Challenge of High-Power Performance of Low-Platinum Proton-Exchange Membrane Fuel Cells. J. Phys. Chem. Lett. *7*, 1127–1137.

3. US Department of Energy (2016). Fuel Cell Technologies Office Multi-Year Research, Development, and Demonstration Plan. Planned Program Activities for 2011-2020. https://www.energy.gov/sites/prod/files/2014/12/f19/fcto_myrdd_full_document.pdf.

4. Song, Z., Norouzi Banis, M., Liu, H., Zhang, L., Zhao, Y., Li, J., Doyle-Davis, K., Li, R., Knights, S., Ye, S., et al. (2019). Ultralow Loading and High-Performing Pt Catalyst for a Polymer Electrolyte Membrane Fuel Cell Anode Achieved by Atomic Layer Deposition. ACS Catal. *9*, 5365–5374.

5. Yarlagadda, V., Carpenter, M.K., Moylan, T.E., Kukreja, R.S., Koestner, R., Gu, W., Thompson, L., and Kongkanand, A. (2018). Boosting Fuel Cell Performance with Accessible Carbon Mesopores. ACS Energy Lett. *3*, 618–621.

6. Banham, D., and Ye, S. (2017). Current Status and Future Development of Catalyst Materials and Catalyst Layers for Proton Exchange Membrane Fuel Cells: An Industrial Perspective. ACS Energy Lett. *2*, 629–638.

7. Chong, L., Wen, J., Kubal, J., Sen, F.G., Zou, J., Greeley, J., Chan, M., Barkholtz, H., Ding, W., and Liu, D.-J. (2018). Ultralow-loading platinum-cobalt fuel cell catalysts derived from imidazolate frameworks. Science *362*, 1276–1281.

8. Escudero-Escribano, M., Malacrida, P., Hansen, M.H., Vej-Hansen, U.G., Velázquez-Palenzuela, A., Tripkovic, V., Schiøtz, J.,

Rossmeisl, J., Stephens, I.E.L., and Chorkendorff, I. (2016). Tuning the activity of Pt alloy electrocatalysts by means of the lanthanide contraction. Science *352*, 73–76.

9. Luo, S., Tang, M., Shen, P.K., and Ye, S. (2017). Atomic-Scale Preparation of Octopod Nanoframes with High-Index Facets as Highly Active and Stable Catalysts. Adv. Mater. *29*, https://doi.org/10.1002/adma.201601687.

10. Li, M., Zhao, Z., Cheng, T., Fortunelli, A., Chen, C.-Y., Yu, R., Zhang, Q., Gu, L., Merinov, B.V., Lin, Z., et al. (2016). Ultrafine jagged platinum nanowires enable ultrahigh mass activity for the oxygen reduction reaction. Science *354*, 1414–1419.

11. Wang, X.X., Swihart, M.T., and Wu, G. (2019). Achievements, challenges and perspectives on cathode catalysts in proton exchange membrane fuel cells for transportation. Nat. Catal. *2*, 578–589.

12. Weber, A.Z., and Kusoglu, A. (2014). Unexplained transport resistances for low-loaded fuel-cell catalyst layers. J. Mater. Chem. A Mater. Energy Sustain. *2*, 17207–17211.

13. Subbaraman, R., Strmcnik, D., Paulikas, A.P., Stamenkovic, V.R., and Markovic, N.M. (2010). Oxygen reduction reaction at three-phase interfaces. ChemPhysChem *11*, 2825–2833.

14. Kocha, S.S., Zack, J.W., Alia, S.M., Neyerlin, K.C., and Pivovar, B.S. (2012). Influence of ink composition on the electrochemical properties of Pt/C electrocatalysts. ECS Trans. *50*, 1475.

15. Liu, C.Y., and Sung, C.C. (2012). A review of the performance and analysis of proton exchange membrane fuel cell membrane electrode assemblies. J. Power Sources *220*, 348–353.

16. Harzer, G.S., Orfanidi, A., El-Sayed, H., Madkikar, P., and Gasteiger, H.A. (2018). Tailoring Catalyst Morphology towards High Performance for Low Pt Loaded PEMFC Cathodes. J. Electrochem. Soc. *165*, F770–F779.

17. Park, Y.-C., Kakinuma, K., Uchida, H., Watanabe, M., and Uchida, M. (2015). Effects of short-side-chain perfluorosulfonic acid ionomers as binders on the performance of low Pt loading fuel cell cathodes. J. Power Sources *275*, 384–391.

18. Kodama, K., Motobayashi, K., Shinohara, A., Hasegawa, N., Kudo, K., Jinnouchi, R., Osawa, M., and Morimoto, Y. (2018). Effect of the Side-Chain Structure of Perfluoro-Sulfonic Acid Ionomers on the Oxygen Reduction Reaction on the Surface of Pt. ACS Catal. *8*, 694–700.

19. Shahgaldi, S., Alaefour, I., and Li, X. (2018). The impact of short side chain ionomer on polymer electrolyte membrane fuel cell performance and durability. Appl. Energy *217*, 295–302.

20. Ngo, T.T., Yu, T.L., and Lin, H.-L. (2013). Influence of the composition of isopropyl alcohol/water mixture solvents in catalyst ink solutions on proton exchange membrane fuel cell performance. J. Power Sources *225*, 293–303.

21. Kim, Y.S., Welch, C.F., Mack, N.H., Hjelm, R.P., Orler, E.B., Hawley, M.E., Lee, K.S., Yim, S.-D., and Johnston, C.M. (2014). Highly durable fuel cell electrodes based on ionomers dispersed in glycerol. Phys. Chem. Chem. Phys. *16*, 5927–5932.

22. Doo, G., Lee, J.H., Yuk, S., Choi, S., Lee, D.-H., Lee, D.W., Kim, H.G., Kwon, S.H., Lee, S.G., and Kim, H.-T. (2018). Tuning the Ionomer Distribution in the Fuel Cell Catalyst Layer with Scaling the Ionomer Aggregate Size in Dispersion. ACS Appl. Mater. Interfaces *10*, 17835–17841.

23. Sharma, R., and Andersen, S.M. (2018). Zoom in Catalyst/Ionomer Interface in Polymer Electrolyte Membrane Fuel Cell Electrodes: Impact of Catalyst/Ionomer Dispersion Media/Solvent. ACS Appl. Mater. Interfaces *10*, 38125–38133.

24. Wang, M., Park, J.H., Kabir, S., Neyerlin, K.C., Kariuki, N.N., Lv, H., Stamenkovic, V.R., Myers, D.J., Ulsh, M., and Mauger, S.A. (2019). Impact of Catalyst Ink Dispersing Methodology on Fuel Cell Performance Using in-Situ X-ray Scattering. ACS Appl. Energy Mater. *2*, 6417–6427.

25. Orfanidi, A., Madkikar, P., El-Sayed, H.A., Harzer, G.S., Kratky, T., and Gasteiger, H.A. (2017). The Key to High Performance Low Pt Loaded Electrodes. J. Electrochem. Soc. *164*, F418–F426.

26. Ott, S., Orfanidi, A., Schmies, H., Anke, B., Nong, H.N., Hübner, J., Gernert, U., Gliech, M., Lerch, M., and Strasser, P. (2020). Ionomer distribution control in porous carbon-supported catalyst layers for high-power and low Pt-loaded proton exchange membrane fuel cells. Nat. Mater. *19*, 77–85.

27. Park, Y.-C., Tokiwa, H., Kakinuma, K., Watanabe, M., and Uchida, M. (2016). Effects of carbon supports on Pt distribution, ionomer coverage and cathode performance for polymer electrolyte fuel cells. J. Power Sources *315*, 179–191.

28. Yarlagadda, V., McKinney, S.E., Keary, C.L., Thompson, L., Zulevi, B., and Kongkanand, A. (2017). Preparation of PEMFC Electrodes from Milligram-Amounts of Catalyst Powder. J. Electrochem. Soc. *164*, F845–F849.

29. Xu, S., Kim, Y., Park, J., Higgins, D., Shen, S.-J., Schindler, P., Thian, D., Provine, J., Torgersen, J., Graf, T., et al. (2018). Extending the limits of Pt/C catalysts with passivation-gas-incorporated atomic layer deposition. Nat. Catal. *1*, 624–630.

30. Klingele, M., Breitwieser, M., Zengerle, R., and Thiele, S. (2015). Direct deposition of proton exchange membranes enabling high performance hydrogen fuel cells. J. Mater. Chem. A Mater. Energy Sustain. *3*, 11239–11245.

31. Gasteiger, H.A., Kocha, S.S., Sompalli, B., and Wagner, F.T. (2005). Activity benchmarks and requirements for Pt, Pt-alloy, and non-Pt oxygen reduction catalysts for PEMFCs. Appl. Catal. B *56*, 9–35.

32. Zihrul, P., Hartung, I., Kirsch, S., Huebner, G., Hasché, F., and Gasteiger, H.A. (2016). Voltage Cycling Induced Losses in Electrochemically Active Surface Area and in H 2 /Air-Performance of PEM Fuel Cells. J. Electrochem. Soc. *163*, F492–F498.

33. Neyerlin, K.C., Gu, W., Jorne, J., and Gasteiger, H.A. (2006). Determination of Catalyst Unique Parameters for the Oxygen Reduction Reaction in a PEMFC. J. Electrochem. Soc. *153*, A1955.

34. Subramanian, N.P., Greszler, T.A., Zhang, J., Gu, W., and Makharia, R. (2012). Pt-Oxide Coverage-Dependent Oxygen Reduction Reaction (ORR) Kinetics. J. Electrochem. Soc. *159*, B531–B540.

35. Moore, M., Putz, A., and Secanell, M. (2013). Investigation of the ORR Using the Double-Trap Intrinsic Kinetic Model. J. Electrochem. Soc. *160*, F670–F681.

36. Wang, J.X., Zhang, J., and Adzic, R.R. (2007). Double-trap kinetic equation for the oxygen reduction reaction on Pt(111) in acidic media. J. Phys. Chem. A *111*, 12702–12710.

37. Baker, D.R., Caulk, D.A., Neyerlin, K.C., and Murphy, M.W. (2009). Measurement of Oxygen Transport Resistance in PEM Fuel Cells by Limiting Current Methods. J. Electrochem. Soc. *156*, B991.

38. Göbel, M., Kirsch, S., Schwarze, L., Schmidt, L., Scholz, H., Haußmann, J., Klages, M., Scholta, J., Markötter, H., Alrwashdeh, S., et al. (2018). Transient limiting current measurements for characterization of gas diffusion layers. J. Power Sources *402*, 237–245.

39. Pang, F.M., Seng, C.E., Teng, T.T., and Ibrahim, M.H. (2007). Densities and viscosities of aqueous solutions of 1-propanol and 2-propanol at temperatures from 293.15 K to 333.15 K. J. Mol. Liq. *136*, 71–78.

40. Vazquez, G., Alvarez, E., and Navaza, J.M. (1995). Surface Tension of Alcohol + Water from 20 to 50 °C. J. Chem. Eng. Data *40*, 611–614.

41. Welch, C., Labouriau, A., Hjelm, R., Orler, B., Johnston, C., and Kim, Y.S. (2012). Nafion in Dilute Solvent Systems: Dispersion or Solution? ACS Macro Lett. *1*, 1403–1407.

42. Shao, M., Peles, A., and Shoemaker, K. (2011). Electrocatalysis on platinum nanoparticles: particle size effect on oxygen reduction reaction activity. Nano Lett. *11*, 3714–3719.

43. Breitwieser, M., Klingele, M., Britton, B., Holdcroft, S., Zengerle, R., and Thiele, S. (2016). The reasons for the high power density of fuel cells fabricated with directly deposited membranes. J. Power Sources *326*, 170–175.

44. Ahluwalia, R.K., Wang, X., and Steinbach, A.J. (2016). Performance of advanced automotive fuel cell systems with heat rejection constraint. J. Power Sources *309*, 178–191.

45. Padgett, E., Yarlagadda, V., Holtz, M.E., Ko, M., Levin, B.D.A., Kukreja, R.S., Ziegelbauer, J.M., Andrews, R.N., Ilavsky, J., Kongkanand, A., et al. (2019). Mitigation of PEM Fuel Cell Catalyst Degradation with Porous Carbon Supports. J. Electrochem. Soc. *166*, F198–F207.

46. Kutz, R.B., Chen, Q., Yang, H., Sajjad, S.D., Liu, Z., and Masel, I.R. (2017). Sustainion Imidazolium-Functionalized Polymers for Carbon Dioxide Electrolysis. Energy Technol. (Weinheim) *5*, 929–936.

47. King, D.M., Spencer, J.A., Liang, X., Hakim, L.F., and Weimer, A.W. (2007). Atomic layer deposition on particles using a fluidized bed reactor with in situ mass spectrometry. Surf. Coat. Tech. *201*, 9163–9171.

48. Tiznado, H., Domínguez, D., Muñoz-Muñoz, F., Romo-Herrera, J., Machorro, R., Contreras, O.E., and Soto, G. (2014). Pulsed-bed atomic layer deposition setup for powder coating. Powder Technol. *267*, 201–207.

49. Poodt, P., Cameron, D.C., Dickey, E., George, S.M., Kuznetsov, V., Parsons, G.N., Roozeboom, F., Sundaram, G., and Vermeer, A. (2012). Spatial atomic layer deposition: a route towards further industrialization of atomic layer deposition. J. Vac. Sci. Technol. A *30*, 010802.

50. Zhang, J., Litteer, B., Coms, F., and Makharia, R.R. (2011). Recoverable Performance Loss Due to Membrane Chemical Degradation in PEM Fuel Cells. ECS Trans. *41*, 1471.

51. Li, J., Xi, Z., Pan, Y.T., Spendelow, J.S., Duchesne, P.N., Su, D., Li, Q., Yu, C., Yin, Z., Shen, B., et al. (2018). Fe Stabilization by Intermetallic $L1_0$-FePt and Pt Catalysis Enhancement in $L1_0$-FePt/Pt Nanoparticles for Efficient Oxygen Reduction Reaction in Fuel Cells. J. Am. Chem. Soc. *140*, 2926–2932.

52. Brodt, M., Wycisk, R., Dale, N., and Pintauro, P. (2016). Power output and durability of electrospun fuel cell fiber cathodes with PVDF and nafion/PVDF binders. J. Electrochem. Soc. *163*, F401–F410.

53. Jia, Q., Caldwell, K., Strickland, K., Ziegelbauer, J.M., Liu, Z., Yu, Z., Ramaker, D.E., and Mukerjee, S. (2015). Improved Oxygen Reduction Activity and Durability of Dealloyed $PtCo_x$ Catalysts for Proton Exchange Membrane Fuel Cells: Strain, Ligand, and Particle Size Effects. ACS Catal. *5*, 176–186.